Available online at www.sciencedirect.com
ScienceDirect
International Journal of Plasticity 23 (2007) 1105–1125
INTERNATIONAL JOURNAL OF Plasticity
www.elsevier.com/locate/ijplas

Effect of oxygen content and microstructure on the thermo-mechanical response of three Ti–6Al–4V alloys: Experiments and modeling over a wide range of strain-rates and temperatures

Akhtar S. Khan *, Rehan Kazmi, Babak Farrokh, Marc Zupan

Department of Mechanical Engineering, University of Maryland Baltimore County, Baltimore, MD 21250, USA

Received 27 August 2006; received in final revised form 6 October 2006
Available online 31 January 2007

Abstract

Results from a series of experiments on three different titanium alloys, under quasi-static and dynamic loading conditions are presented. The Ti–6Al–4V titanium alloys include the ELI version and two with higher oxygen contents. The strain-rates are varied from 10^{-6} to 3378 s^{-1} while observations are made at temperatures from 233 to 755 K. The alloys initial and deformed photomicrographs and various deformation mechanisms responsible for the induced plastic deformation, are presented and discussed. Differences in the responses of these alloys are observed in terms of thermal softening, work hardening, and strain-rate and temperature sensitivities. The Khan–Huang–Liang (KHL) model is used to effectively simulate the observed responses obtained from these experiments. The model, with the constants determined from these experiments, is then used to predict strain-rate jump experimental results, and also high temperature dynamic experiments for one of the alloys; the predictions are found to be very close to the observations.

Keywords: Dynamic compression; Thermal softening; Compression split-Hopkinson bar; Titanium alloys; Strain rate sensitivity

* Corresponding author. Tel.: +1 410 455 3301; fax: +1 410 455 1052.
E-mail address: khan@umbc.edu (A.S. Khan).

0749-6419/$ - see front matter © 2006 Published by Elsevier Ltd.
doi:10.1016/j.ijplas.2006.10.007

1. Introduction

Since the emergence of titanium and titanium alloys in the early 1950s, they have become important materials for aerospace, energy, and chemical processing industries. These alloys are used chiefly for parts requiring good corrosion resistance, moderate strength up to 588 K, and are lightweight. Titanium alloys, especially Ti–6Al–4V, an $\alpha + \beta$ alloy, is attractive to designers because of its high specific strength and stiffness, good formability, reasonable ductility and ability to withstand high temperatures and resistance to corrosion. Because of these properties this alloy is utilized in aero-engine, gas turbines and other weight critical applications.

The conventionally processed, relatively expensive Ti–6Al–4V alloy has found applications in aerospace components; its high strength and stiffness to weight ratio have improved the total vehicle range and maneuverability. However, this alloy has limited implementation in ground applications where the costs outweigh performance improvements. This has resulted in the development of relatively cheaper Ti–6Al–4V alloys using a single electron beam melting process, resulting in a slightly high interstitial content but improved ductility. The increased ductility is advantageous in armor applications, including ceramic tiles encapsulated in these titanium alloys (Montgomery and Wells, 2001). Several experimental studies have been carried out on these materials to evaluate their performances under different loading conditions, and to investigate their yield behaviors (Follansbee and Gray, 1989; Lee and Lin, 1997, 1998; Da Silva and Ramesh, 1997; Lesuer, 2000; Nemat-Nasser et al., 2001; Majorell et al., 2002).

Follansbee and Gray (1989) studied the deformation mechanism of Ti–6Al–4V titanium alloy in as-received, solution treated and solution treated-aged conditions. They concluded that only at very high strain rates ($\sim$5000 s^{-1}) the mechanical twins develop; at strain rates below these levels planar slip is the most dominant deformation mechanism. Lee and Lin (1997, 1998) studied the high temperature dynamic deformation of these alloys. They observed that the effect of temperature on yielding is more prominent at higher temperatures, but is independent of strain rate.

Nemat-Nasser et al. (2001) performed experiments on a commercially available and hot isostatically pressed (HIP) Ti–6Al–4V titanium alloy. Dynamic recrystallization at high strain rates and also dynamic strain aging at higher temperatures were observed. Majorell et al. (2002) studied the response of this alloy at low to moderate strain rates and moderate to high temperatures. They observed that the temperature sensitivity of the flow stress was reduced with increasing the temperature.

The mechanical properties of Ti–6Al–4V alloys are heavily influenced by impurities and heat treatment, making it imperative that the alloys behaviors are linked to microstructure, phase constituents, and processing history. Unalloyed titanium exists mainly in two forms; α-titanium (hcp structure) at room temperature, and β-titanium (bcc structure) at elevated temperatures. The α phase (primary and secondary) is more dominant at temeratures ranging from 300 to 800 K, while the amount of β phase starts to increase thereon and is almost totally β-phase at about 1270 K, known as the β transus temperature (Majorell et al., 2002). The α phase is much harder than the β phase, so the drop in strength with the temperature rise results from increase in the β content. Alternatively, formability increases as the phase transforms from α to β. Various alloying agents are added to titanium, stabilizing the two phases. Aluminum, oxygen, nitrogen, and carbon are α stabilizers, while vanadium, iron and manganese are β stabilizers.

Deformation in the alloy is accommodated by planar slip in the lower temperature range (<500 K) with slip occurring on the basal, prismatic and the pyramidal planes. At temperatures below 800 K, increase in Al content causes the transformation of primary α into secondary α. When deformed, the secondary α phase has a higher dislocation density than primary α and a smaller grain size. These observations suggest that it is harder than the primary α phase (Picu and Majorell, 2002). Studies by Conrad and Wang (1978), on high purity titanium, and the titanium with 7.4% wt. Al, revealed an increase in the flow stress with the addition of Al content. The increase in flow stress is attributed to higher Al concentration, enhancing the production of the secondary α phase, making the alloy harder. The study also verified an inverse dependency of strength to the grain size for the material with titanium's flow stress obeying the Hall–Petch relation (Conrad, 1984). Strain hardening in the alloy was attributed to be more from the presence of the lamellar Widmanstätten microstructure of the secondary α phase. However, De Meester et al. (1975) noticed that the addition of aluminum did not alter the rate controlling mechanism and the aluminum contributed only to the athermal components of the flow stress. The study showed that the rate controlling mechanism was the thermally activated component overcoming of the interstitial solute atoms. They also found that, over a temperature range of 300–800 K the flow stress vs. temperature curve of α-titanium was nearly parallel to that of Ti–6Al–4V alloy of similar interstitial content. The study concluded that the alloying elements did not influence the temperature sensitivity in this temperature range, and the interaction of dislocations with interstitial impurities (C, N, O and H) was more responsible for the behavior. They also concluded that the deformation kinetics and related parameters for the Ti–6Al–4V alloy were the same as those for unalloyed titanium.

Chichili et al. (1998) found that twinning, an important deformation mechanism, occurred at all temperatures below 773 K for α-titanium; at high strain rates the density of twins increases with deformation. Paton et al. (1976) observed no twinning for Ti–6Al–4V alloys even at low temperatures of 100 K, suggesting that increase in aluminum content inhibited twinning. However, at room temperature, some twinning was observed by Follansbee and Gray (1989) at strain rate of 5000 s^{-1} in grains which were larger than the average size.

Conrad et al. (1973) proposed an equivalent oxygen content ($O_{eq} = O + 2N + 0.75C$), capturing the effect of dislocations-impurity interaction on the yield strength of the material. They noted that the strengthening of the alloy from these interstitials was dependent on, in decreasing order, carbon, oxygen and nitrogen; effect of hydrogen in most cases was nominal. Majorell et al. (2002) studied the deformation characteristics and response of a textured and untextured Ti–6Al–4V alloy rod manufactured by Allvac Inc. (P.O. Box 5030 Monroe, NC 28111-5030). This study was performed over a strain-rate range of 10^{-3}–10 s^{-1} and a temperature range of 650–1345 K. The equivalent oxygen content of the specimen was 0.206% and the average grain size was 20 μm. They did not observe any dynamic strain aging at any of the investigated temperatures or strain rates. They also included the equivalent oxygen content and aluminum impurities in the thermal stress component and the grain size effect in the athermal stress component of the yield behavior model.

This manuscript presents a study to compare the mechanical responses of three Ti–6Al–4V alloys with different equivalent oxygen contents, deformed at low and high temperatures, and strain rates from 10^{-6} to 3378 s^{-1}. Subsequently, the capability of the modified

KHL model (Khan and Liang, 1999; Khan et al., 2004) to capture the behavior of three titanium alloys is examined. Comparisons of the KHL model correlations and predictions with the Johnson–Cook model (Johnson and Cook, 1983) for one of the alloys studied here, as well as those investigated by Nemat-Nasser et al. (2001) and Macdougall and Harding (1999) can be found in Khan et al., 2004. The reader is referred to papers by Abed and Voyiadjis (2005) and Uenishi and Teodosiu (2004), for other modeling approaches.

2. Experimental procedure

2.1. Material

Three titanium alloys with different chemical compositions given in Table 1 were investigated in this study. The effect of impurities on the alloys stress-strain responses under different loading conditions was explored. The alloys were as-received condition plates. Quasi-static specimens were machined to a diameter of 12.7 mm and length of 19.05 mm. Specimens for the dynamic Kolsky bar testing were machined to discs with 10.16 mm diameter and 5.08 mm thickness. The loading direction (axis of cylinders) in all specimens was in the thickness direction of the plate. Care was taken during the machining of specimens to avoid introducing plastic work hardening on the surface. This was done by making the last three machining cuts very small. The alloys have been designated as number 1, 2 and 3 with equivalent oxygen contents of 0.229%, 0.152% and 0.222% wt., respectively. Alloys 1 and 3 were manufactured using single electron beam melting process, resulting in higher oxygen contents than the extra-low interstitial (ELI) alloy 2.

2.2. Microstructure evaluation

The microstructures of the alloys were evaluated before and after deformation using a scanning electron microscope (SEM). The specimens were cut along the loading axis and polished using different grits of silicon carbide paper starting from 240, 400, 600, 800, and finishing with 2400. A final polish was conducted using a Struers DP-Plus micro cloth with slurry of 0.3 μm alumina, achieving mirror-like finish. Samples were etched with Kroll's reagent (a solution of 1% HF, 2% HNO_3 and 97% distilled H_2O), for ~5 min until the microstructure was revealed.

Photomicrographs of the initial microstructures are given in Figs. 1 and 2 for alloys 2 and 3, respectively. They reveal an alpha-beta type microstructure with the α phase appearing as the bright or low contrast regions. Alloy 3 was subjected to different annealing (~1230 K) and cooling processes, resulting in a higher amount of transformed β content (dark regions). Its microstructure consists of the hcp α grains and a transformed β with

Table 1
Chemical composition of the three Ti–6Al–4V alloys

Material	Al	V	Fe	Y	H	N	O	C	Ti	O_{eq}
Alloy 1	6.26	4.16	0.14	<0.0003	0.0031	0.008	0.178	0.047	REM	0.229
Alloy 2	6.30	3.86	0.18	<0.0003	0.0026	0.003	0.112	0.045	REM	0.152
Alloy 3	5.97	4.09	0.15	<0.0003	0.0041	0.008	0.174	0.043	REM	0.222

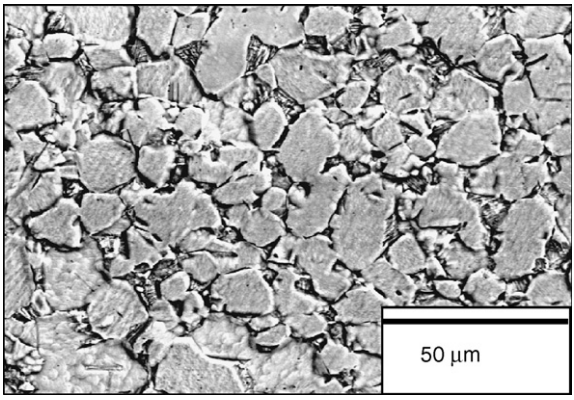

Fig. 1. Undeformed microstructure for alloy 2.

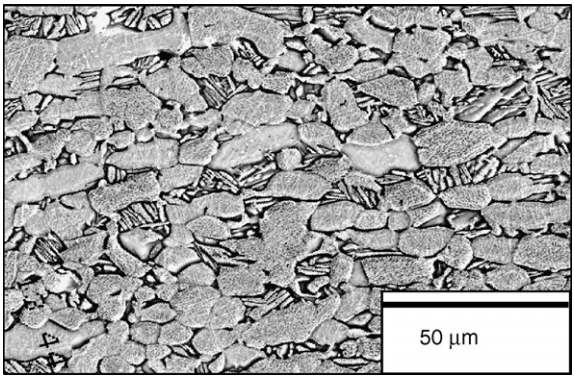

Fig. 2. Undeformed microstructure for alloy 3.

a lamellar Widmanstätten structure dispersed between these primary globular α grains. The higher annealing temperature along with higher rate of cooling is responsible for the increased transformed β content as compared to the other alloys. The percentage of lamellar transformed β is lower in alloy 2 relative to alloy 3. However, the aluminum content, which is an α phase stabilizer, is higher in alloys 1 and 2 than alloy 3. Also, the average grain size for all of the titanium alloys was approximately 8 μm, which was calculated using the intercept method (ASTM International E 112, 1996).

2.3. Quasi-static experiments at room and different temperatures

All the quasi-static experiments were performed in compression. For the room temperature experiments, high elongation uniaxial strain gages were mounted diametrically opposite to each other at the center of each specimen. The measured strains using strain gages were corrected for Wheatstone bridge non-linearity and gage factor variation before conversion into plastic strains (Huang and Khan, 1991). The interfaces between the loading platens and the specimen were lubricated using Teflon sheets and grease, achieving uniformity in deformation, avoiding barreling of the specimen and maintaining a uniform,

uniaxial stress state. Specimens were subjected to different strain rates, ranging from 10^{-6} to 1 s^{-1} on an MTS servo hydraulic axial/torsional testing system. The 1 s^{-1} experiment was performed as a load–unload–reload experiment in increments of 5% strain with a 30-min interval between each consecutive loading, to obtain an isothermal response of the material.

The compressive stress-strain responses were measured for experiments at temperatures ranging from 233 to 755 K at a strain rate of 10^{-4} s^{-1} for alloys 1 and 2, and 10^{-3} s^{-1} for alloy 3. Alumina platens were attached to the grips of the testing system using Vascomax C-350 fixtures to thermally isolate the samples. A thermocouple was cemented directly to the center of the specimen to directly monitor the sample temperature throughout the experiment. The specimen was then subjected to a pre-defined temperature field; once the desired temperature was reached, it was held constant for 30 min, establishing equilibrium conditions throughout the specimen. The MTS linear voltage displacement transducer (LVDT) supplied stroke data while the force was measured by a 2200 kN load cell. Displacement data measured by this method include machine compliance, deformation of the ceramic bars and those contributed by the utilized lubricants. These were then subtracted from the total displacement to obtain sample's net deformation.

For the low temperature experiments, a chamber containing dry ice was placed around the specimen. The specimen temperature was monitored using the same technique as previously described. The specimen temperature was reduced to 233 K and remained steady during the test. Corrections for the displacement were performed similar to that of high temperature experiments.

2.4. Dynamic experiments at room and different temperatures

Dynamic experiments on the alloys were performed using the compression Split-Hopkinson Pressure Bar (SHPB) technique. The diameter of these bars, made from Vascomax C-350 steel, was 12.7 mm. The disc specimen was sandwiched between the incident and transmitted bars with the interfaces of the bars lubricated with appropriate grease to reduce friction and to maintain a uniform stress state in the specimen. Strain gages were mounted on the bars diametrically opposite to each other and positioned such that the incident, reflected and transmitted waves were recorded without any interaction among the waves. Strain signals were measured using a Nicolet 440 oscilloscope through a potentiometer circuit. The stresses and the corresponding strains in the specimen were calculated using the incident, reflected and transmitted waves signals. For more details on the split-Hopkinson bar technique and the associated calculations the reader is referred to Follansbee (1979) and Khan and Liang (1999).

During the high temperature dynamic experiments, specimens were heated to predetermined temperatures. High temperature grease was applied to the interfaces between the specimen and the bars. Thermocouples were cemented to the outside surfaces of the specimens to monitor the temperature directly; once the test temperature was achieved the sample was held constant for ~15 min insuring temperature uniformity throughout the specimen. The temperature of the Hopkinson bars was kept at approximately room temperature using forced cooling to avoid change in the elastic modulus of the incident and the transmitted bars.

During the high strain rate experiments most of the heat generated by the plastic work is entrapped within the specimen, artificially softening the responses; this process is known

as thermal softening. Thermal softening is a function of the specific heat capacity at constant pressure, mass density and the amount of deformation in the specimen. A small portion of the generated heat is consumed to change the microstructure and enabling dislocation mobility. Thus, high strain-rate deformation is adiabatic and there is a significant increase in the temperature of the specimen during the experiment. The effect of thermal softening is significant and cannot be neglected. The temperature rise in the specimen can be estimated by the following equation (Khan and Liang, 1999):

$$\Delta T = \frac{\beta}{\rho C_{\mathrm{p}}} \int_0^{\varepsilon} \sigma(\varepsilon)\, \mathrm{d}\varepsilon. \tag{1}$$

In this study, the fraction of plastic work, β, converted to heat is taken to be 0.9, implying that 90% of the plastic work done during the deformation is assumed to be converted to heat, causing a rise in the temperature of the specimen. ρ and C_{p} are the mass density and the specific heat at constant pressure for the alloy, respectively. The density for the titanium (Ti–6Al–4V) alloys is 4428 kg/m^3 (Lesuer, 2000) and the specific heat capacity at constant pressure for the alloys can be expressed as a function of temperature of the material (Military Handbook, 1998)

$$C_{\mathrm{p}} = 559.77 - 0.1473T + 0.00042949T^2 \ \mathrm{J/(kg\ K)} \quad (278\ \mathrm{K} < T < 1144\ \mathrm{K}). \tag{2}$$

This relation is used to convert the adiabatic experimental response at high strain rates to the corresponding isothermal behavior.

3. Experimental results

The stress-strain responses from the compression experiments on the alloys are given in Figs. 3–6 and Figs. 8, 9. For alloy 1, five different strain-rate experiments were performed

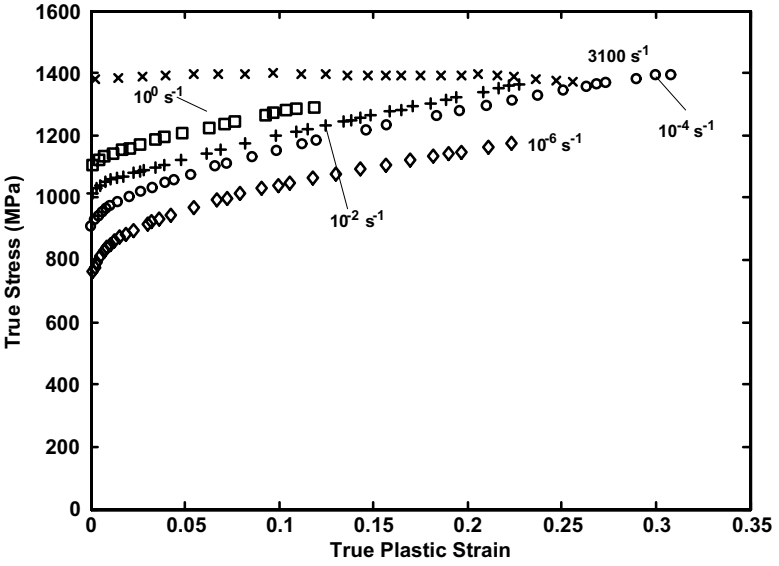

Fig. 3. True stress–strain response at different strain rates and room temperature for the titanium alloy 1.

ranging from 10^{-6} s^{-1} to dynamic strain rate of 3100 s^{-1}at room temperature (Fig. 3). The material behavior was found to be strain rate sensitive; it shows a nonlinear work hardening response at the lower deformation levels transitioning to an almost linear response at higher deformation levels. Also, there is a slight reduction in work hardening rate with

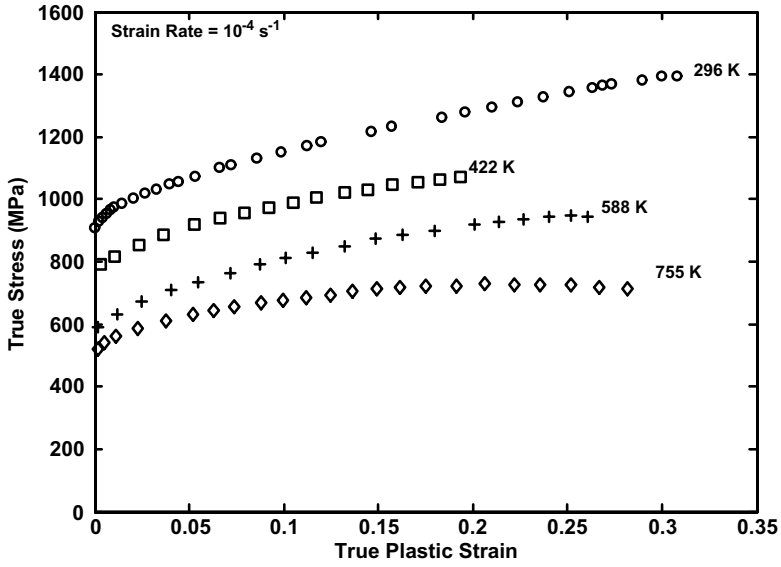

Fig. 4. True stress–strain response at different temperatures at the strain rate of 10^{-4} s^{-1} for the titanium alloy 1.

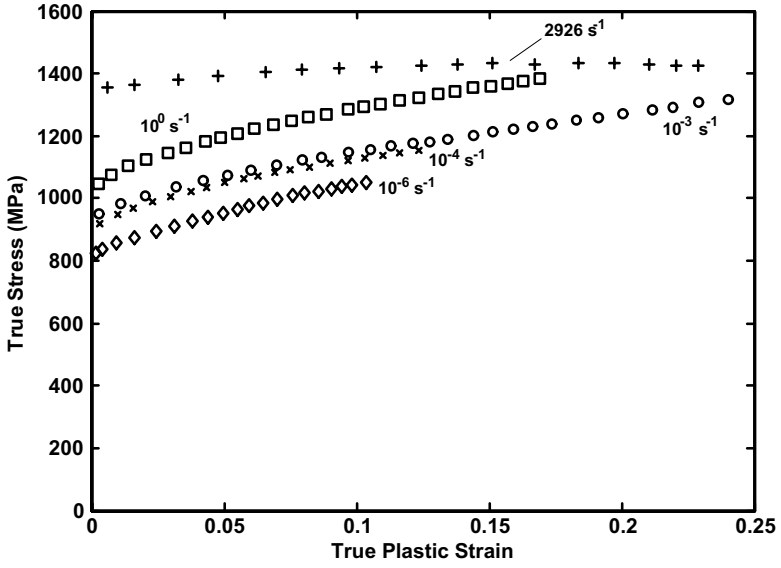

Fig. 5. True stress–strain response at different strain rates and room temperature for the titanium alloy 2.

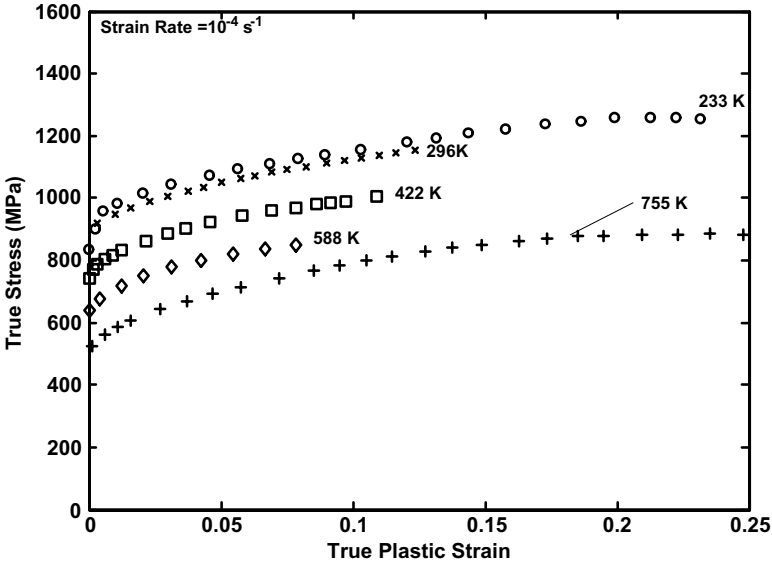

Fig. 6. True stress–strain response at different temperatures at the strain rate of 10^{-4} s^{-1} for the titanium alloy 2.

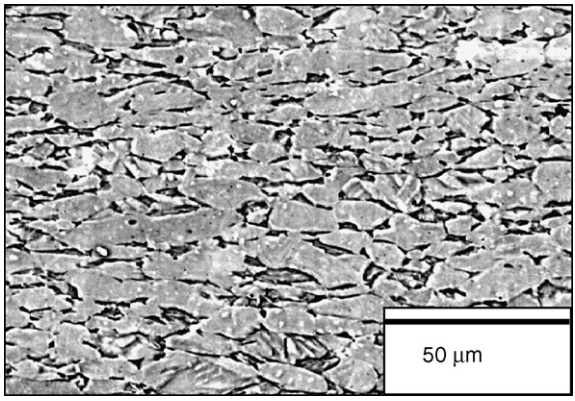

Fig. 7. Deformed microstructure of alloy 2 for an experiment performed at 296 K and 10^{0} s^{-1} strain rate at 18% strain showing the globular α with dispersed β along the grain boundaries.

increasing strain rates in the quasi-static loading regime. There is no or little work hardening effect in the adiabatic dynamic experiment due to thermal softening. The observed response of the material is also a non-linear function of temperature (Fig. 4). The increase in test temperature causes reduction in the flow stresses. A slight decrease in work hardening rate behavior is observed as the temperatures and/or strain level are increased. This observation is consistent with other studies on the alloy (Majorell et al., 2002; Lee and Lin, 1997). The flow stress in the alloy was found to be more sensitive to temperature of the material than to the strain rate. This result is similar to those obtained by Nemat-Nasser et al. (2001) on a similar alloy.

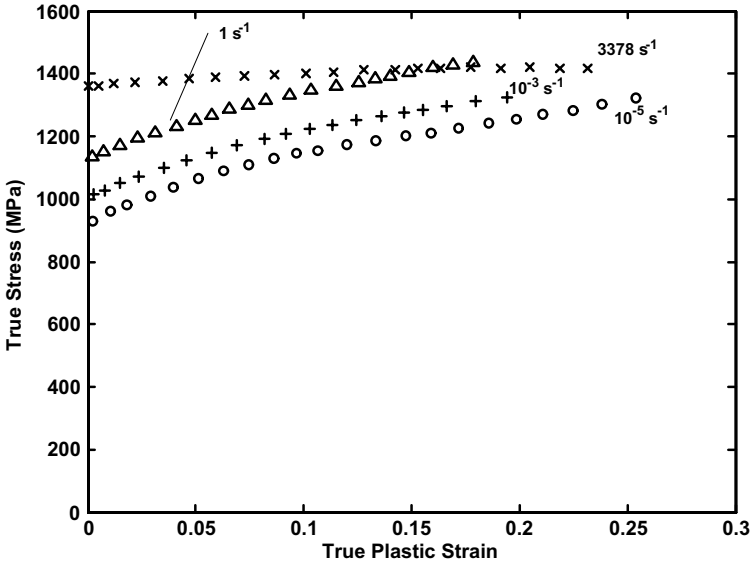

Fig. 8. True stress–strain response at different strain rates and room temperature for the titanium alloy 3.

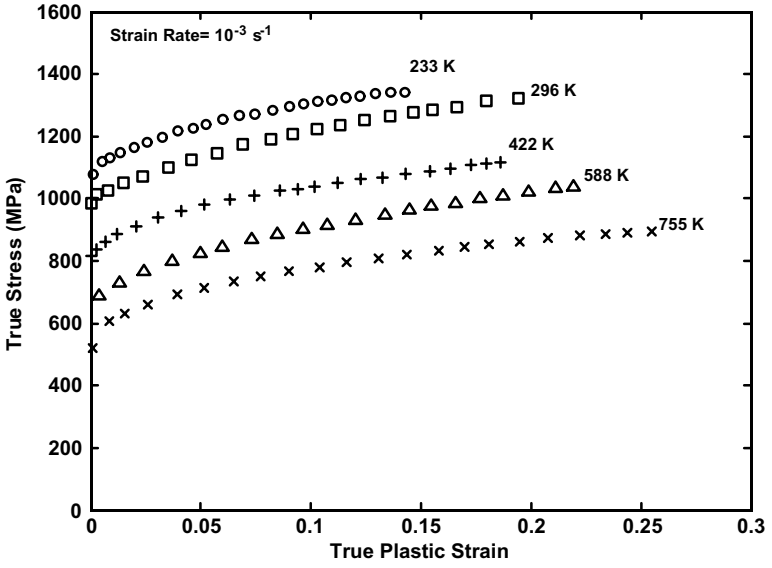

Fig. 9. True stress–strain response at different temperatures at the strain rate of 10^{-3} s^{-1} for the titanium alloy 3.

For alloy 2 experiments were performed at strain rates ranging from 10^{-6} to 2926 s^{-1} and are shown in Fig. 5. Quasi-static experiments at different temperatures were performed at 233, 422, 588 and 755 K (Fig. 6). All of these experiments were executed well below beta transus temperature (~1270 K) to ensure that the material did not change phase during

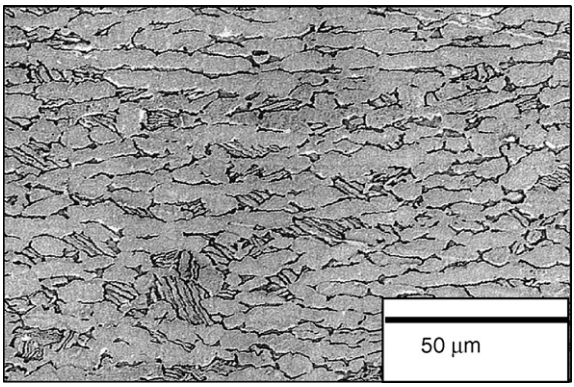

Fig. 10. Deformed microstructure of alloy 3 for an experiment performed at 422 K and 10^{-3} s^{-1} strain rate at 20% strain showing the globular α with dispersed transformed β (Widmanstätten structure).

the experiments. The photomicrograph of the alloy 2 sample deformed at room temperature and at a strain rate of 1 s^{-1} is shown in Fig. 7. The deformed microstructure shows elongated hcp α grains. The transformed β grains in the sample displayed no apparent change in the substructure and this was independent of the level of deformation or loading condition.

Similarly, different strain-rate and temperature experiments were performed for alloy 3. Room temperature experiments, shown in Fig. 8, covered a range of strain rates from 10^{-5} to 3378 s^{-1}. Experiments at different temperatures (233, 422, 588 and 755 K) on this alloy were performed at a strain rate of 10^{-3} s^{-1}, Fig. 9. A photomicrograph of the alloy 3 deformed microstructure is shown in Fig. 10. This sample was deformed at a temperature of 422 K and at the strain rate of 10^{-3} s^{-1}. The microstructure shows elongated hcp α grains similar to alloy 2 and is consistent with the observations of other researchers (Follansbee and Gray, 1989).

Photomicrographs of deformed samples under dynamic loading conditions at various temperatures for this alloy are also shown in Fig. 11. These samples show significant elongation of grains at high strain rates and different temperatures. The percentages of primary α and transformed β were measured using digital imaging processes. The measurement revealed a decreasing transformed β content with increasing test temperature for dynamically deformed samples. This result is attributed to the energy generated in the samples causing recrystallization of the transformed β into globular α grains. Elongation of these recrystallized grains is identified in the sample deformed at high strain rates and 715 K temperature.

Twinning, an important deformation mechanism found in unalloyed samples of titanium, was not observed in the alloys tested in this study. The result is consistent with the study by Follansbee and Gray (1989), where the authors found deformation twins only at very high strain rate (5000 s^{-1}) experiments. The behavior is attributed to a reduced dislocation mobility requiring high stresses for deformation, resulting in development of deformation twinning at very high strain rate and low temperatures. However, in the case of low strain rates and high temperatures, dislocation motion is the dominating component in the deformation mechanism of the alloys through planar slips with negligible amounts of twin deformation.

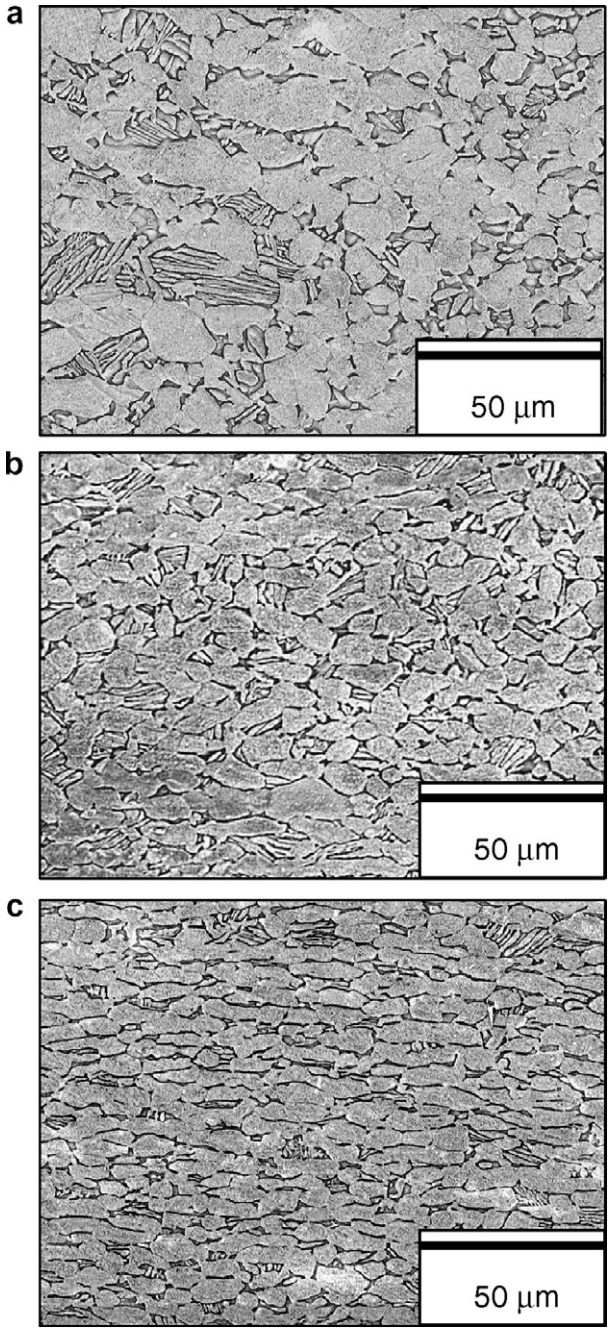

Fig. 11. Deformed samples of alloy 3 at high strain rates ($\sim$2300 s^{-1}) and different temperatures: (a) at 296 K, (b) at 422 K and (c) at 715 K (compression along vertical direction).

4. Modeling procedure

The KHL model utilizes a systematic method of determining initial material constants (see Khan and Liang, 1999), which are used as input in a program to obtain refined material constants employing an optimization technique; the model is then used to predict the material response over a wide range of strain rates and temperatures. There are six material constants, which define the material behavior with respect to the yield strength, strain hardening, strain rate sensitivity, temperature sensitivity and strain hardening sensitivity to strain rate. The model is robust and has proven to be capable of capturing complex material behaviors such as decreasing work hardening with increasing strain rate, etc. More detail of this model is given in Khan et al. (2004). The KHL constitutive equation is given as:

$$\sigma = \left[A + B\left(1 - \frac{\ln \dot{\varepsilon}}{\ln D_0^{\mathrm{p}}}\right)^{n_1} \varepsilon_{\mathrm{p}}^{n_0}\right]\left(\frac{\dot{\varepsilon}}{\dot{\varepsilon}^*}\right)^{c}\left(\frac{\mathrm{T_m} - T}{T_{\mathrm{m}} - T_{\mathrm{ref}}}\right)^{m}, \tag{3}$$

where σ is the true (Cauchy) stress and ε^{p} is the true plastic strain. T_{m}, T, T_{ref} are melting, current, and reference temperatures, respectively. $D_0^{\mathrm{p}} = 10^6\ \mathrm{s}^{-1}$ (arbitrarily chosen upper bound strain rate) and $\dot{\varepsilon}^* = 1\ \mathrm{s}^{-1}$ (reference strain rate, at a reference temperature of T_{ref}, usually room temperature, at which material constants A,B and n_0 are determined). $\dot{\varepsilon}$ is the current strain rate. n_1, C and m are additional material constants. For Ti–6Al–4V alloys, the melting temperature was taken to be 1933 K (Nemat-Nasser et al., 2001). The reference temperature was the constant room temperature for experiments at 296 K.

The material constants for this model were determined using several uniaxial quasi-static and dynamic room temperature experimental results at different strain rates, also high and low temperature experimental results at one strain rate. This method as described above, provides one with a set of initial material constants which can be used as initial input into an algorithm utilizing an optimization procedure though a least square method to obtain a set of more refined material constants. The dynamic data before being input to the optimization scheme was converted into an equivalent isothermal data by calculating the instantaneous temperature rise in the material at any strain level using Eq. (1), and calculating the stress increment for that temperature rise to obtain corresponding isothermal stress response. Subsequently, the determined material constants were used to predict a strain rate jump experiment, which was performed separately for each alloy. The strain rate jump experiment included at least two different strain rates in the quasi-static regime followed by a dynamic regime strain rate. It is noted that, for all the presented results the strain rate jump experiments were not used to calculate the material constants, but used as a verification of the model's capabilities.

5. Correlations with the constitutive model

5.1. Correlations and predictions for alloy 1

The data correlations obtained for room temperature experiments are shown in Fig. 12 along with the experimental observations. The material constants obtained for this alloy, using the MATLAB software, utilizing the least square method with constrained optimization, are shown in Table 2. The constants, depicting the strain rate sensitivity of work hardening n_1 and the strain rate sensitivity parameter C, were kept identical for all three

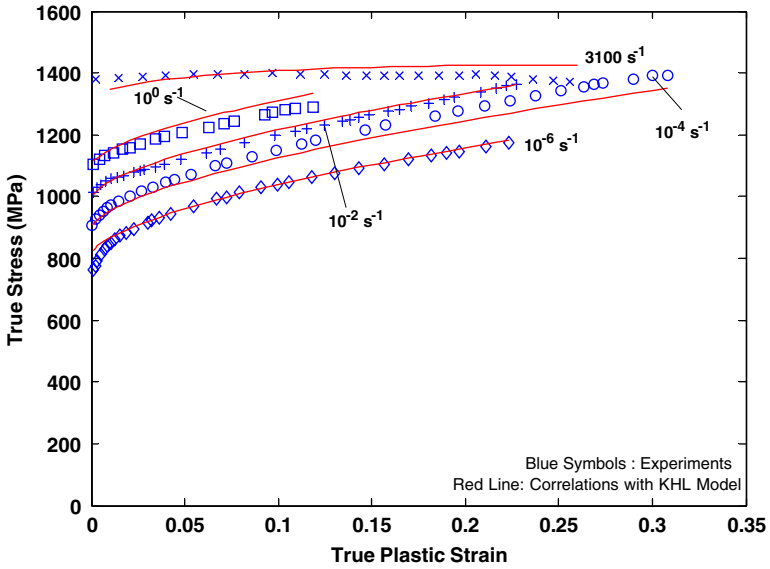

Fig. 12. KHL model correlations with the room temperature (296 K) response of alloy 1 at different strain rates.

alloys. In spite of imposing these extra constraints in the optimization procedure, the KHL model was able to successfully correlate with the material response over large strains and displaying excellent capability in simulating decreased work hardening behavior with increasing strain rate. In all figures the predictions/correlations from the model are shown by solid lines. The various correlations for different temperatures can be seen in Fig. 13. Here also, the model correlates reasonably well with the data. Further, in Fig. 14, a room temperature strain rate jump experiment from 10^{-5} to 10^{-1} s^{-1}, followed by another jump at a dynamic strain rate of 1816 s^{-1}, is predicted closely by the model.

5.2. Correlations and predictions for alloy 2

The various material constants for this alloy are given in Table 2. Here again, the two material constants, n_1 and C, were kept identical as it was assumed that the heat treatment and slight changes in composition only change the constants A, B, n_0 and m. Results of the correlations can be seen in Fig. 15. The model is in good agreement with the experimentally observed response during the quasi-static room temperature experiments throughout the plastic deformation regime. The dynamic response is also close to the correlations, including the replication of the reduced work hardening throughout the deformation. The model correlations for observed responses at different temperatures are given in

Table 2
KHL model material constants determined for the three Ti–6Al–4V alloys

	A (MPa)	B (MPa)	n_1	n_0	C	m
Ti–6Al–4V Alloy 1	1100	857.5	0.5455	0.6086	0.02204	1.6236
Ti–6Al–4V Alloy 2	988	747.1	0.5455	0.3986	0.02204	1.2214
Ti–6Al–4V Alloy 3	1069	874.8	0.5455	0.4987	0.02204	1.3916

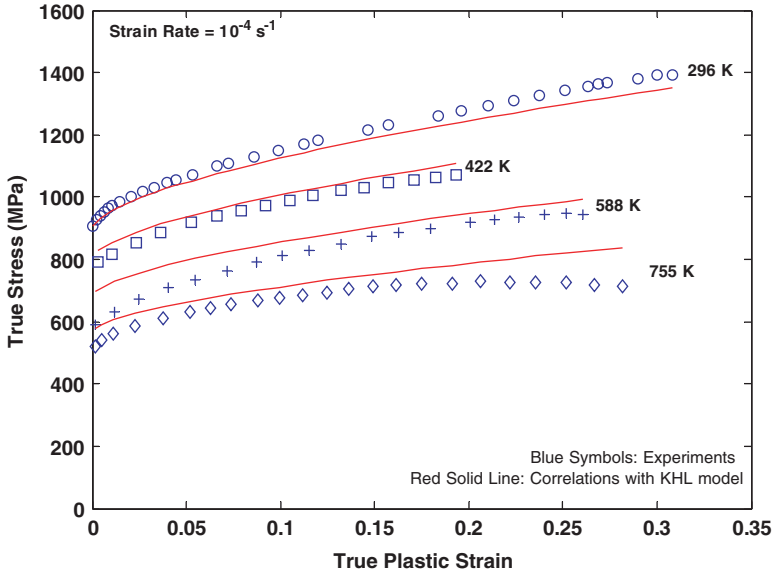

Fig. 13. KHL model correlations with the observed response of alloy 1 at different temperatures and at the constant strain-rate 10^{-4} s^{-1}.

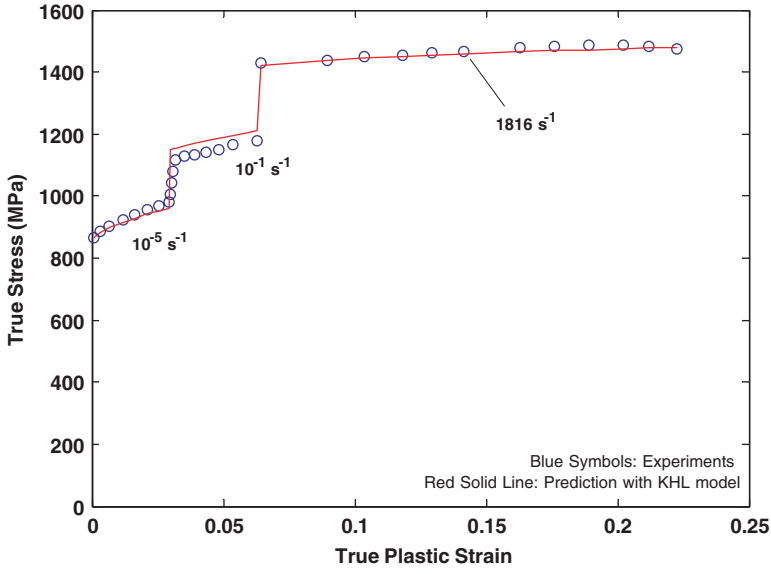

Fig. 14. KHL model predictions with the observed response of alloy 1 during a strain-rate jump experiment at room temperature (296 K). Dynamic predictions are adiabatic.

Fig. 16. The model is again in good agreement with the experimentally observed responses for the low (233 K) as well as other high temperature experiments. Similar to alloy 1, a strain rate jump experiment was performed on this alloy from 10^{-5} to 1 s^{-1} and then back

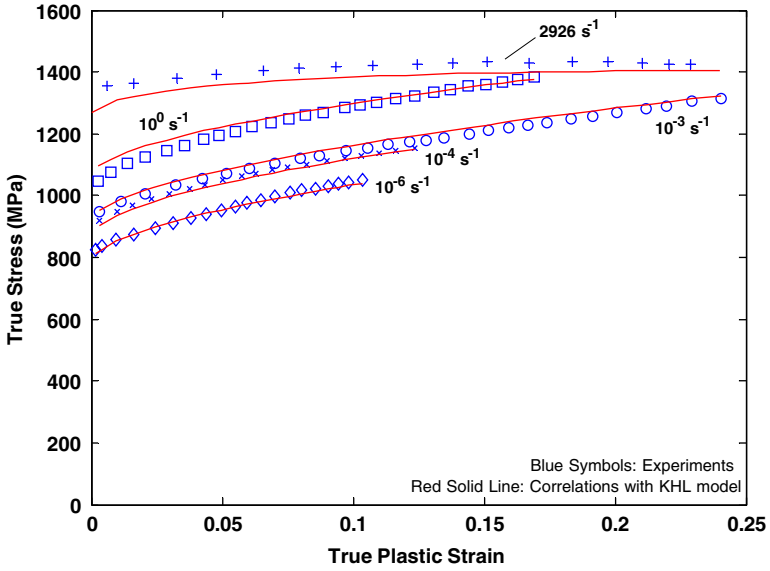

Fig. 15. KHL model correlations with the room temperature (296 K) response for alloy 2 at different strain rates.

to $10^{-5}\,s^{-1}$, before performing a dynamic experiment on the same specimen. In predictions, the responses were assumed adiabatic for the strain rate of $1\,s^{-1}$ and also for the dynamic strain rate regime portion of the experiment. The model predictions are in good agreement for all strain rates and to all levels of strain as shown in Fig. 17.

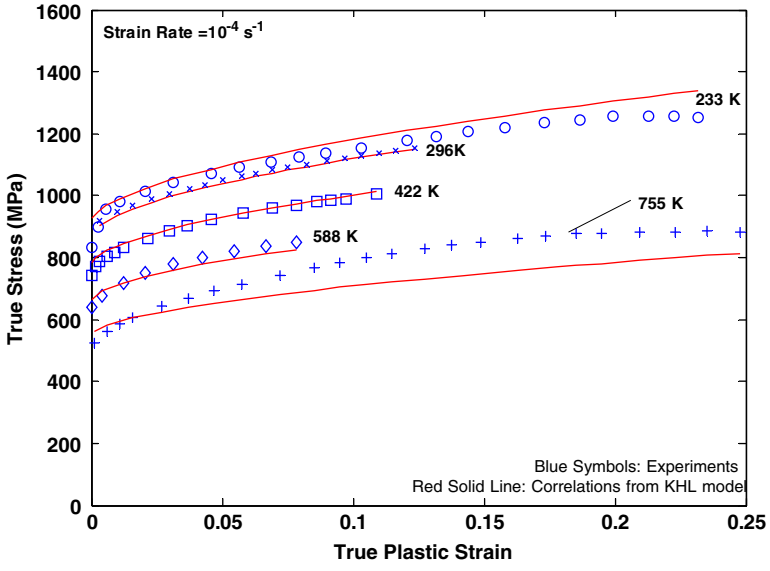

Fig. 16. KHL model correlations with the observed response of alloy 2 at different temperatures at constant strain-rate $10^{-4}\,s^{-1}$.

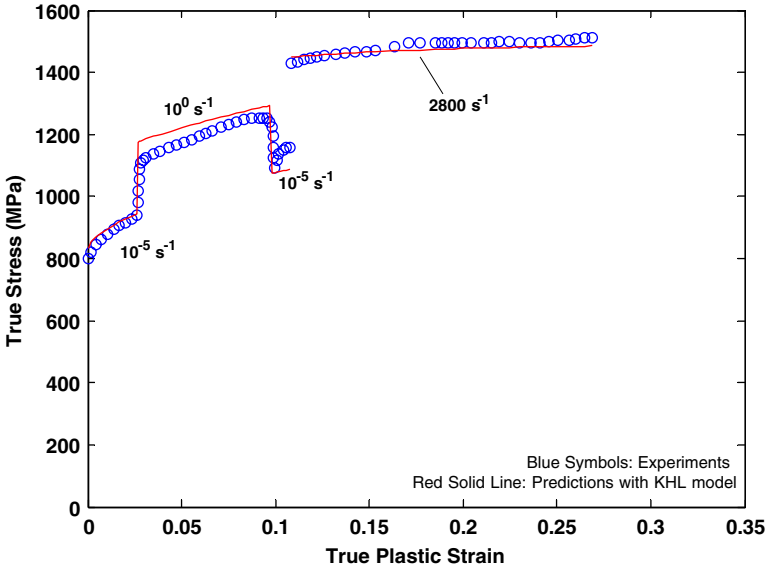

Fig. 17. KHL model predictions with the observed response of alloy 2 during a strain-rate jump experiment at room temperature (296 K). Dynamic predictions are adiabatic.

5.3. Correlations and predictions for alloy 3

The response modeling for alloy 3 was performed similar to the other two alloys. The material constants thus obtained after refinement of the initial constants, are given in Table 2. The measured responses during four quasi-static and dynamic experiments at room temperature are shown in Fig. 18 along with the correlations obtained for this alloy showing excellent agreement. As with the other two alloys subjected to dynamic loading, the isothermal values were converted into adiabatic responses before comparing them with the adiabatic dynamic results. The correlations with the experimental results at different temperatures and at the strain rate of 10^{-3} s^{-1} are provided in Fig. 19. The observations and the model correlations are again in good agreement with each other for all temperatures. A strain rate jump experiment was performed at a strain rate of 10^{-5}–10^{-1} s^{-1}, followed by a dynamic strain rate experiment at 1700 s^{-1} on the same specimen. Predictions were performed and the experimental results along with the predictions are compared in Fig. 20. As, in all the previous cases the predictions are in good agreement with the observed results. The prediction for the strain rate of 10^{-1} s^{-1} was converted into corresponding adiabatic response, before comparison, as there was a temperature increase noticed in the specimen during the experiment. Similarly, dynamic strain rate regime prediction was also converted in order to obtain the adiabatic response.

Predictions for high strain rate experiments are also shown for different temperatures in Fig. 21. The predictions were converted to adiabatic responses so they could be plotted along with the experimental results. The predicted response is again in excellent agreement with the experimental observations.

Overall, the correlations and the model predictions were very close to measured experimental responses for a large range of strain rates and temperatures. Further, it was

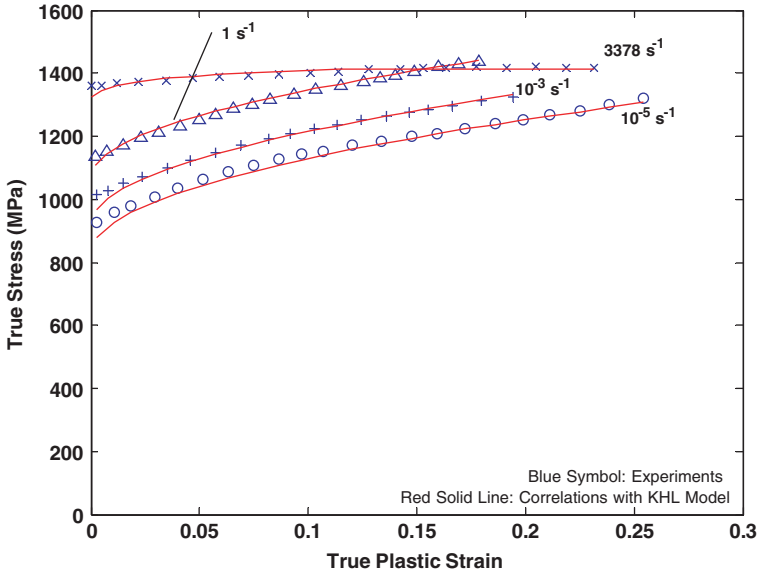

Fig. 18. KHL model correlations with the room temperature (296 K) response for alloy 3 at different strain rates (published data: Khan et al., 2004).

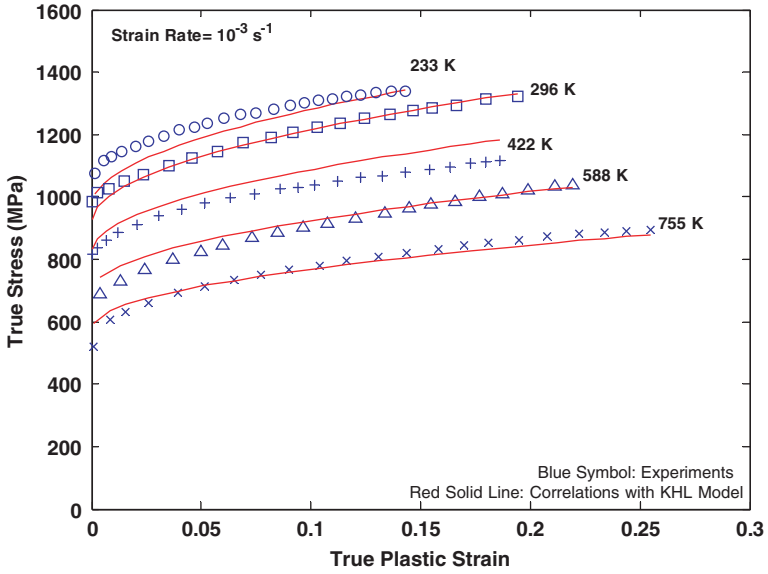

Fig. 19. KHL model correlations with the observed response of alloy 3 at different temperatures at constant strain-rate 10^{-3} s^{-1} (published data: Khan et al., 2004).

observed from the measured responses that alloys 1 and 3 had a higher flow stress as compared to the alloy 2. This is attributed to the fact that the interstitial solute content or the equivalent oxygen content (O_{eq}), which is known to strengthen the alloy, is higher in these

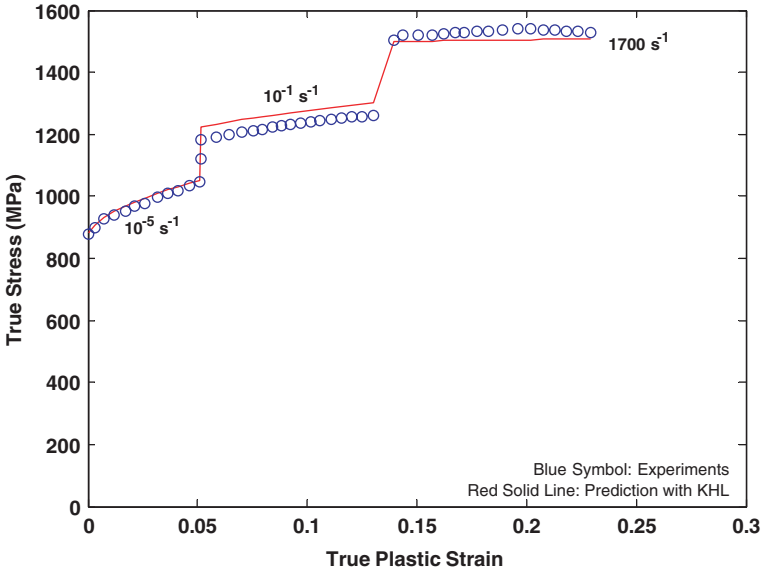

Fig. 20. KHL model predictions with the observed response of alloy 3 during a strain-rate jump experiment at room temperature (296 K). Dynamic predictions are adiabatic (published data: Khan et al., 2004).

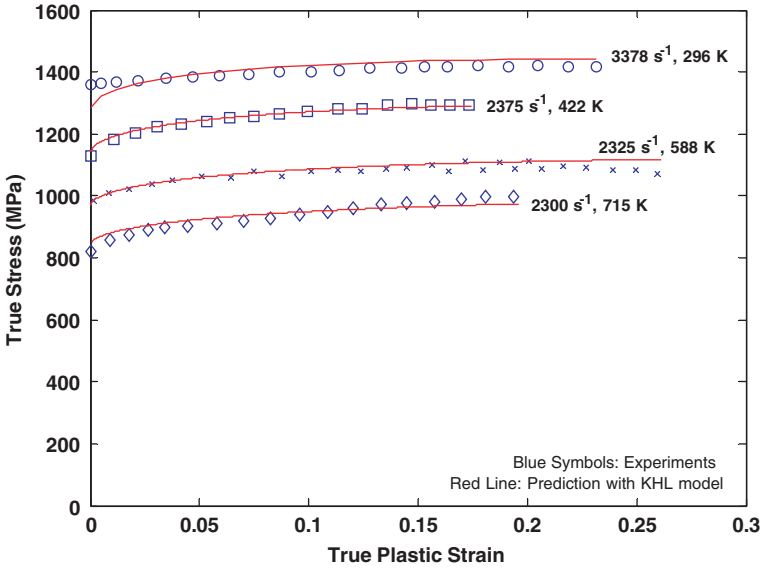

Fig. 21. KHL model predictions with the observed response of alloy 3 at high strain rates and different temperatures. All the predictions are adiabatic.

alloys (Okazaki and Conrad, 1982). Alloy 2 is the ELI grade alloy and has a lower flow stress response during various experiments. The work hardening in the alloys 1 and 3 were found to be quite similar but higher than that of alloy 2; this is evident from the material

constants (B and n_0) listed in Table 2. However, responses of the alloys at different temperatures are slightly different; this characteristic is also highlighted in Table 2, where the three alloys have different temperature sensitivity parameters. From the above observations it can be concluded that the interstitial impurities have significant effects on the flow stress and work hardening responses of the alloys; these additions also affect the temperature sensitivity of the alloys. This is consistent with the findings of other researchers (De Meester et al., 1975). Also, the interstitial content has no apparent effect on the work hardening sensitivity of strain rate, as well as the overall strain rate sensitivity of the material.

6. Conclusions

In the present paper, the quasi-static and dynamic responses of three titanium alloys were studied in a systematical manner over wide ranges of strain rates and temperatures. The alloys were found to be more sensitive to change in temperature than strain rate. The KHL model was utilized to model the observed behavior of these three different alloys over these ranges. The model was found to be fairly accurate to closely capture all the important features observed for these alloys. Material constants of the KHL model were determined for all three alloys; previously determined values were used for predictions of the observed material response in strain-rate jump experiments (all alloys) and high strain rate experiments at different temperatures for alloy 3 to show the applicability of the model. Two of the six constants were kept identical for all three alloys, suggesting that the strain rate sensitivity and the strain rate effect on the work hardening of the alloys were independent of the interstitial content and the small differences in the initial microstructures of these alloys. Further, the yield strength, work hardening and the temperature sensitivity were found to be somewhat different for these alloys; thus it was concluded that the amount of interstitial content and the initial microstructure had been responsible for these variations in the observed responses.

Acknowledgments

The first author is grateful for the funding of this project by the Army Research Office under awards DAAD19-01-1-0635 & W911NF-05-1-0208, under the direction of Dr. Bruce LaMattina (Solid Mechanics Program). The first author is also thankful to Dr. Douglas Templeton, Team Leader of Emerging Technologies at US Army TARDEC for funding of the project and guidance. Various help and comments of Dr. Raj Rajendran at the Army Research Office are also gratefully acknowledged. Also, the assistance in performing some experiments by former graduate students, Jennifer Baker and Robert Matteson, is greatly appreciated.

References

Abed, F.H., Voyiadjis, G.Z., 2005. Plastic deformation modeling of AL-6XN stainless steel at low and high strain rates and temperatures using a combination of bcc and fcc mechanisms of metals. International Journal of Plasticity 21 (8), 1618–1639.

ASTM International, 1996. Standard Test Methods for Determining the Average Grain Size. Designation E 112-96. July 1996, PA, USA.

Chichili, D.R., Ramesh, K.T., Hemker, K.J., 1998. The high strain rate response of alpha-titanium: experiments, deformation mechanisms and modeling. Acta Materialia 46 (3), 1025–1043.

Conrad, H.M., Doner, M., de Meester, B., 1973. Critical review deformation and fracture. International Conference on Titanium, Proceedings of Titanium Science and Technology. Massachusetts Institute of Technology, Boston, p. 969.

Conrad, H., Wang, K., 1978. Solid solution strengthening of titanium by aluminum at low temperatures. In: 5th International Conference on Strength of Materials and Alloys, 1978, pp. 1067–1072.

Conrad, H., 1984. Plastic flow and fracture of titanium at low temperatures. Cyrogenics (June), 293–304.

Da Silva, M.G., Ramesh, K.T., 1997. The rate-dependent deformation and localization of fully dense and porous Ti-6Al-4V. Materials Science and Engineering A 232 (1–2), 11–22.

De Meester, B., Doner, M., Conrad, H., 1975. Deformation kinetics of the Ti–6Al–4V alloy at low temperatures. Metallurgical Transactions A 6, 1975–1965.

Follansbee, P.S., 1979. High strain rate compression testing. American Society for Metals, Mechanical Testing, Metals Handbook, ninth ed., vol. 8, pp. 190–205.

Follansbee, P.S., Gray III, G.T., 1989. An analysis of the low temperature, low and high strain-rate deformation of Ti–6Al–4V. Metallurgical Transactions A 20 (5), 863–874.

Huang, S., Khan, A.S., 1991. On the use of electrical-resistance metallic foil strain gages for measuring large dynamic plastic deformation. Experimental Mechanics 31, 122–125.

Johnson, G.R., Cook, W.H., 1983. A constitutive model and data for metals subjected to large strains, high strain rates and high temperatures. In: Proceedings of the Seventh International Symposium on Ballistic, The Hague, The Netherlands, 1983, p. 541.

Khan, A.S., Liang, R., 1999. Behaviors of three BCC metal over a wide range of strain rates and temperatures: experiments and modeling. International Journal of Plasticity 15 (9), 1089–1109.

Khan, A.S., Suh, Y.S., Kazmi, R., 2004. Quasi-static and dynamic loading responses and constitutive modeling of titanium alloys. International Journal of Plasticity 20, 2233–2248.

Lee, W.S., Lin, M.T., 1997. The effects of strain rate and temperature on the compressive deformation behavior of Ti–6Al–4V alloy. Journal of Metal Processing Technology 71, 235–246.

Lee, W.S., Lin, C.F., 1998. Plastic deformation and fracture behavior of Ti–6Al–4V alloy loaded with high strain rate under various temperatures. Materials Science and Engineering A 241, 48–59.

Lesuer, D.R., 2000. Experimental investigations of material models for Ti–6Al–4V titanium and 2024-T3 aluminum. Final Report, DOT/FAA/AR-00/25, US Department of Transportation, Federal Aviation Administration.

Macdougall, D.A.S., Harding, J., 1999. A constitutive relation and failure criterion for Ti–6Al–4V alloy at impact rates of strain. Journal of the Mechanics and Physics of Solids 47 (5), 1157–1185.

Majorell, A., Srivatsa, S., Picu, R.C., 2002. Mechanical behavior of Ti–6Al–4V at high and moderate temperatures – Part I: experimental results. Materials Science and Engineering A 326 (2), 297–305.

Military Handbook, Metallic Materials and Elements for Aerospace Vehicle Structures, MIL-HDBK-5H, DOD and FAA, 1998.

Montgomery, J.S., Wells, M.G.H., 2001. Titanium armor applications in combat vehicles. JOM 53 (4), 29–32.

Nemat-Nasser, S., Guo, Wei-Guo, Nesterenko, Vitali F., Indrakanti, S.S., Gu, Ya-Bei, 2001. Dynamic response of conventional and hot isostatically pressed Ti–6Al–4V alloys: experiments and modeling. Mechanics of Materials 33 (8), 425–439.

Okazaki, K., Conrad, H., 1982. Mechanisms of plastic deformation and superplasticity. Titanium and Titanium Alloys: Scientific and Technology Aspects 1, 429–466.

Paton, N.E., Baggerly, R.G., Williams, J.C., 1976. AFOSR Final Report. Rockwell International.

Picu, R.C., Majorell, A., 2002. Mechanical behavior of Ti–6Al–4V at high and moderate temperatures – Part II: constitutive modeling. Materials Science and Engineering A 326, 306–316.

Uenishi, A., Teodosiu, C., 2004. Constitutive modeling of the high strain rate behavior of interstitial-free steel. International Journal of Plasticity 20 (4–5), 915–936.